Polymer Bulletin (2019) 76:1697–1715
https://doi.org/10.1007/s00289-018-2463-2

ORIGINAL PAPER

Conducting polymer polypyrrole and titanium dioxide nanocomposites for photocatalysis of RR45 dye under visible light

Ljerka Kratofil Krehula[1] · Jasmina Stjepanović[1] · Martina Perlog[1] · Stjepko Krehula[2] · Vanja Gilja[1] · Jadranka Travas-Sejdic[3] · Zlata Hrnjak-Murgić[1]

Received: 18 January 2018 / Revised: 6 July 2018 / Accepted: 23 July 2018 / Published online: 28 July 2018

Abstract

The interest is given on the preparation of nanocomposites of titanium dioxide (TiO_2) with conducting polymer polypyrrole (PPy) because the resulting composites possess enhanced photocatalytic activity under visible light in comparison with pure TiO_2 photocatalyst. In such composite, there is a synergistic activity of the components. It is very important to optimize the synthesis conditions in order to obtain PPy/TiO_2 composites with the optimal thickness of conductive polymer layer on TiO_2 and minimal possible aggregation of particles. PPy/TiO_2 composites were characterized by Fourier transform infrared spectroscopy, X-ray powder diffraction, UV–Vis spectroscopy, scanning electron microscopy and transmission electron microscopy. The photocatalytic efficiency of the samples was determined by following the decomposition of Reactive Red 45 dye under UV and visible light, which was monitored by UV–Vis spectroscopy (as a change in absorbance of wavelength at 542 nm). The results show enhanced photocatalytic efficiency of the samples under visible light.

Keywords Polypyrrole · Titanium dioxide · Nanocomposite · Photocatalysis · Visible light

✉ Ljerka Kratofil Krehula
krehula@fkit.hr

✉ Zlata Hrnjak-Murgić
zhrnjak@fkit.hr

[1] Faculty of Chemical Engineering and Technology, University of Zagreb, Marulićev trg 19, P.O. Box 177, 10000 Zagreb, Croatia

[2] Division of Materials Chemistry, Ruđer Bošković Institute, P.O. Box 180, 10002 Zagreb, Croatia

[3] School of Chemical Sciences, University of Auckland, Auckland, New Zealand

Introduction

Photocatalysis utilizing solar energy for water purification by degradation of organic pollutants at lower cost and energy consumption remains a challenge for industrial applications [1]. During the past decades, many researches have been focused on developing novel photocatalyst with enhanced photocatalytic efficiency like oxide-based semiconductors, in particular [2–4]. Despite many good properties of TiO_2 (it is non-toxic, chemically and biologically stabile and easily available catalyst), the greatest shortage of TiO_2 catalysts is its high band gap ($E_g = 3.2$ eV) that limits its photoactivity in the visible light region. In response to this disadvantage, much work has been done to improve its photoactivity under sunlight, like doping or surface modification of TiO_2 by conductive polymers [1, 5–9]. The main issue of current research is to consider the extension of the light absorption spectrum to the visible region, facilitating the use of sunlight as an inexpensive energy for photocatalytic processes. The conducting polymers seemed interesting materials with p-conjugated double bonds that have been attracted much attention. Among them particular good conducting polymer is polypyrrole (PPy) and its structure attracted considerable interests due to its good environmental stability, facile synthesis, higher conductivity and promising commercial applications. Conducting polymers with extending conjugated electron systems act as stable photosensitizers injecting electrons into the conduction band of TiO_2 (due to their π conjugated electrons). Under irradiation, electrons are injected from the conducting polymer and react with oxygen to form the oxidizing $O_2^{-\cdot}$ superoxide radical. Nanostructured conjugated polymers are appearing as new energy materials for various applications in fuel cells and solar cells, but photocatalytic activity studies of conducting polymers are still scarce. Their main advantages are low-cost, facile synthesis, excellent electrochemical and electrical activity and high carrier mobility. Although the process of chemical synthesis is simple, the key role is to create suitable structure—properties relationship with functional properties. It includes versatility in terms of monomer functionality and reaction conditions while the main disadvantage is the lack of control over the structure and molecular weight of the polymer product [10]. For example, chemical oxidative polymerization of pyrrole is a suitable technique to obtain highly electrically conducting polypyrrole (PPy) in a powdery form but does not reach the desired conductivity values shown by high-quality electrochemically prepared PPy thin films [2, 3]. The stability and the electrical conductivity of PPy synthesized by chemical oxidative polymerization of pyrrole depend strongly upon the reaction conditions. There are many typical parameters such as temperature, type of the oxidant, solvent, concentration, reactant stoichiometry and reaction time that are important. The in situ synthesis of PPy with TiO_2 presence additionally reflects on the structure—properties relationship due to the interaction of conducting polymer and semiconductor.

In this work we demonstrate the photocatalytic activity of composites consisted of conjugated polymer polypyrrole prepared by chemical oxidative synthesis in the presence of the TiO_2. It was necessary to achieve the appropriate

structure of PPy conductive polymer that can activate TiO_2 under VIS light and establish the synergistic effect. Finally, this composite represents very efficient composite photocatalyst for the degradation of Reactive Red 45 (RR45) azo dye under ultraviolet irradiation and under visible light. Furthermore, we show that these photocatalysts are very stable even after repeated photocatalysis cycle.

Experimental

Materials

Titanium dioxide (TiO_2, P-25, Degussa) Evonik, ≥ 99.5%, nanopowder, 21 nm particle size, pyrrole monomer (Py, 99%, Acros organics), ferric chloride ($FeCl_3$, Sigma-Aldrich) and sodium chloride (NaCl, Merck KGaA) were used. Commercial organic dye C.I. Reactive Red 45 dye (RR45) Ciba-Geigy, Basel, was used. All the reagents were analytical grade and used as received, without further purification. Milli-Q deionized water (conductivity < 1 μS cm^{-1}) was used for the preparation of the dye solution.

Synthesis of PPy/TiO_2 composite photocatalysts

Titanium dioxide/polypyrrole (PPy/TiO_2) composites were synthesized by the chemical polymerization from pyrrole monomer in the presence of TiO_2 nanoparticles and ferric chloride ($FeCl_3$) as an oxidant. First, a solution of pyrrole monomer was prepared in a 0.5 M sodium chloride solution where monomer and oxidant concentrations were kept at ratio of 1:1, and a ratio of polypyrrole: titanium dioxide was 1:100. The polymerization conditions were: a temperature of 5 °C maintained by adding ice to an aqueous bath and time of synthesis was 90, 180, and 270 min with a continuous mixing on a magnetic stirrer (250 rpm).

Techniques

FTIR spectra were obtained using PerkinElmer Spectrum One FTIR spectrometer with the range of 4000–650 cm^{-1} using ATR technique.

Diffuse reflectance UV–Vis-NIR spectra were obtained at 20 °C using a Shimadzu UV–Vis-NIR spectrometer (model UV-3600) equipped with an integrated sphere. Barium sulfate was used as reference.

X-ray powder diffractometer APD 2000 (CuKa radiation, graphite monochromator, NaI-TI detector) manufactured by Ital Structures (G.N.R. s.r.l., Novara, Italy) was used. Potassium bromide (Sigma-Aldrich, 99% trace metals basis) was used as an internal standard. The Rietveld refinements of X-ray powder diffraction (XRD) data were performed using the MAUD program [11].

Scanning electron microscopy (SEM) images (magnifications 2000×) were obtained using a scanning electron microscope TESCAN VEGA 3 SEM at 10 kV.

Before recording samples were applied to the adhesive tape on the sample holder and then their surfaces were coated with a very thin layer of gold.

A JEOL thermal field emission scanning electron microscope (FESEM, model JSM-7000F) was used for the observation of particle morphology at higher magnifications. The FESEM was connected to the Oxford Instruments EDS/INCA 350 energy-dispersive X-ray analyzer for elemental analysis. The specimens were not coated with an electrically conductive surface layer.

Transmission electron microscopy (TEM) images were obtained by transmission electron microscope (FEI Philips C12, 120 kV). The samples were prepared by cutting by diamant knife on Leica EM UC6 microtome. Camera TEM CCD Gatan 791 Bioscan was used for scanning.

Thermogravimetric analysis (TGA) of samples was performed using TA Instruments Q500 analyzer. The results were obtained in a temperature range from 25 to 800 °C at a heating rate of 10 °C min^{-1} under nitrogen atmosphere.

Photocatalysis

The experiments were performed with the waste water containing 30 mg dm^{-3} of Reactive Red 45 azo dye with 1 g dm^{-3} of synthesized PPy/TiO_2 composite photocatalyst and pure TiO_2 for the comparison. The reactions were run with 100 cm^3 of waste water suspension while the pH value was varied from 4, 6.6, to 11. At given irradiation time intervals, aliquot of about 3 cm^3 was sampled, filtered through a 0.45 μm membrane filter to remove the remaining particles. The filtrates were analyzed by recording the absorption of RR45 dye at a wavelength of 542 nm using UV–Vis spectrophotometer, PerkinElmer Lambda EZ 201 spectrophotometer. The irradiation source was Pen-Ray UVP lamp (UVA region: 315–400 nm), and for solar irradiation the source was solar simulator Oriel Newport (Osram XBO 450 W lamp).

In all experiments, the reaction system was stirred in the dark for 30 min to achieve adsorption/desorption equilibrium before irradiation. The photodegradation efficiency was estimated by determination of the concentration (C) of dye after a certain irradiation time where C_0 was used as initial value before irradiation; C_t is a value of dye concentration after certain period of irradiation. The extent of RR45 dye mineralization during the photocatalysis was determined on the basis of total organic carbon (TOC) content; measurements were taken using TOC analyzer, TOC-VCPN 5000 A, Shimadzu.

Results and discussion

FTIR spectroscopy

Fourier transform infrared spectroscopy (FTIR) spectroscopy was used to characterize PPy/TiO_2 composites obtained by in situ synthesis of PPy and the time of polymerization was varied (90, 180 and 270 min), Fig. 1. Spectra reveal characteristic vibration bands for both PPy and TiO_2, which are consistent with the

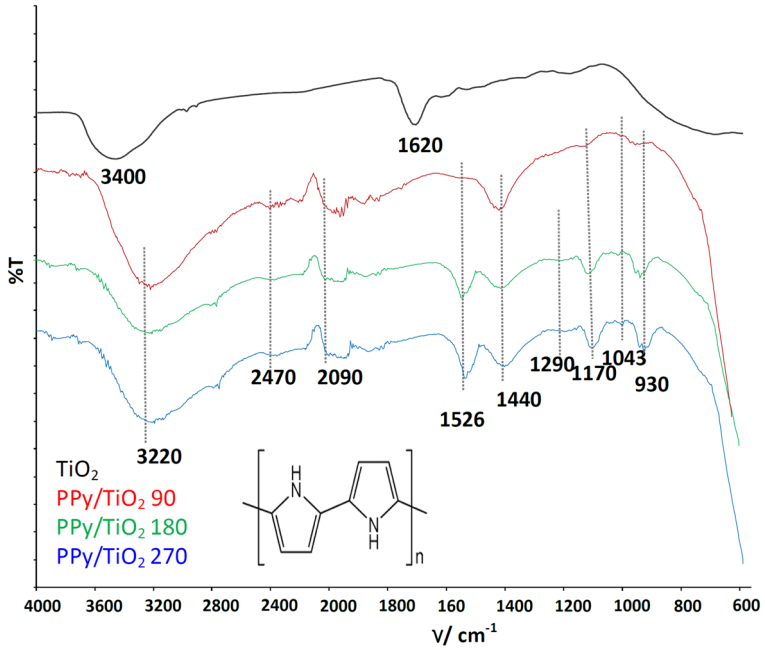

Fig. 1 FTIR spectra of TiO_2 and synthesized PPy/TiO_2 composites

literature [12, 13]. The broad band at about 3400 cm^{-1} is assigned to stretching vibrations of hydroxyl group (–OH) and the band at about 1620 cm^{-1} corresponds to deformative vibration of Ti–OH (the adsorbed water on the TiO_2 surface). The absorption bands that appear in the low-frequency region of spectra located in the range 450–850 cm^{-1} characteristic of a Ti–O–Ti symmetric stretching vibration mode and of Ti–O vibration are partially detected due to restriction of the instrument scanning region. The FTIR spectra of PPy/TiO_2 composites indicates also characteristic PPy bond vibrations at 1526 cm^{-1} characteristic vibration of C=C and C=N bonds in the polypyrrole ring and peak of the low intensity at 1440 cm^{-1} corresponds to =C–CH and –CH in-plane deformation and 930 cm^{-1} out-of-plane deformation. The absorbance at 1043 cm^{-1} corresponds to the C–N in-plane and at 1290 and 1170 cm^{-1} corresponds to out-of-plane deformations. At 3220 cm^{-1} the vibrations of the N–H bonds are observed, while the doping state of PPy is characterized by absorption peaks at approximately 2100, 1170 and 930 cm^{-1} [14]. Also, the appearance of peaks in the wavelength range from 2000 to 2500 cm^{-1} corresponds to the N–C=O bonds [15] due to Ti–O–C=N and Ti–O=C–N structures as results of PPy and TiO_2 interactions. The interaction between TiO_2 and PPy vibrations bands are explained through bordering and shifting of peaks to higher wave number like peaks at 3220, 1526, 1440 and 1290 cm^{-1}, indicating the strong interaction on the interface [16].

X-ray powder diffraction

X-ray powder diffraction was used to analyze TiO_2 and PPy/TiO_2 composites. To reveal a phase structure of TiO_2 sample, Rietveld refinement was carried out (Fig. 2). The results show that the mass ratio of anatase in the sample is 87.6%, while the mass ratio of rutile is 12.4%.

The average size of the crystallites in TiO_2 sample is about 24 nm, and it is calculated from the width of the anatase diffraction line 101 using Scherrer equation [17].

$$\tau = \frac{K\lambda}{\beta \cos \Theta}$$

XRD analysis of PPy/TiO_2 composites reveals the existence of TiO_2 crystal phases of anatase (*A*) and rutile (*R*) in all samples (Fig. 3). It can be noticed that the modification of TiO_2 by PPy does not change the crystallization of the neat TiO_2.

XRD analysis also shows the presence of the halite (*H*), i.e., sodium chloride. Its presence is explained due to its use in a preparation of $FeCl_3$ solution.

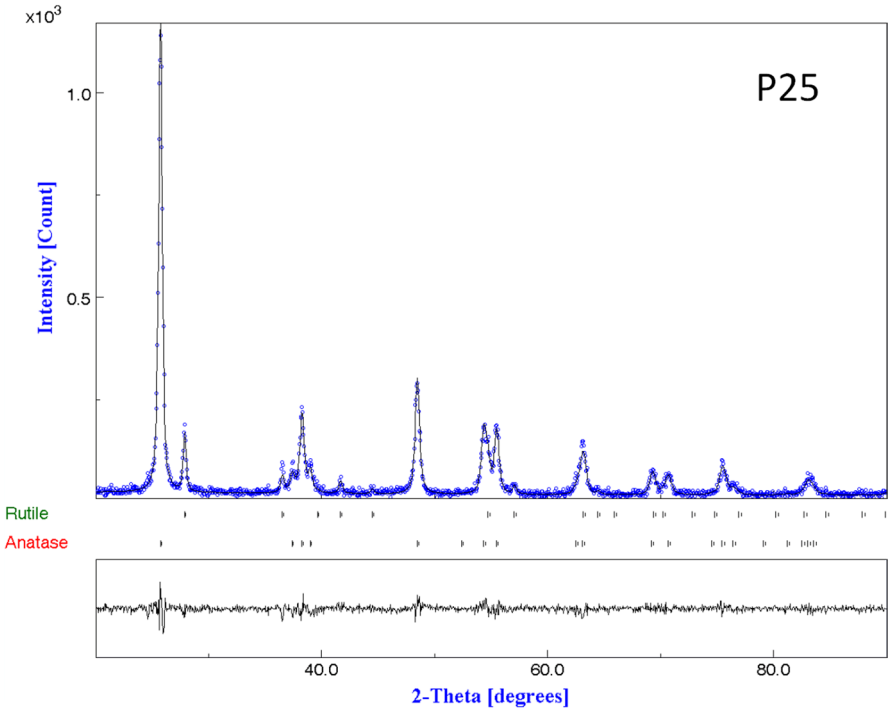

Fig. 2 XRD difractogram of pure TiO_2 (P25)

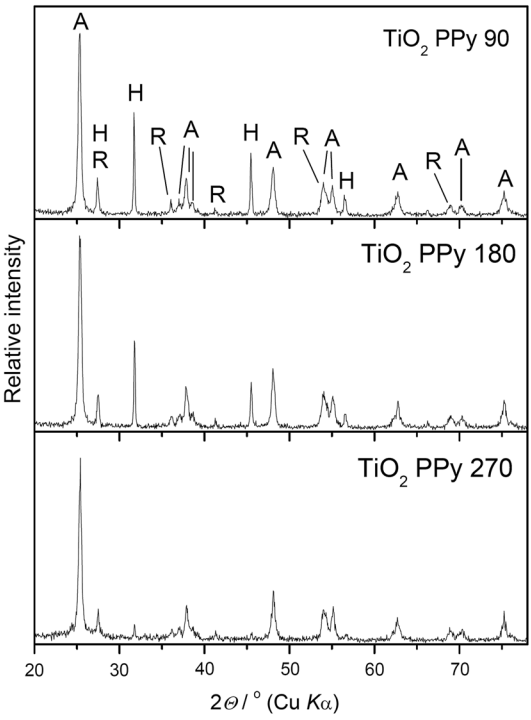

Fig. 3 XRD difractograms of synthesized PPy/TiO_2 composites

TG analysis

Thermal decomposition of the PPy/TiO_2 composites was investigated by TGA in the nitrogen atmosphere to indicate the possible differences in PPy structure of the in situ synthesized composites (Fig. 4). The TG curves in Fig. 4a suggest that the mass loss of PPy polymer occurred in temperature range from 120 to 680 °C. Further, it can be also seen that char residue is decreasing with increase in the PPy concentration since PPy content was totally burned out during the heating process indicating mainly TiO_2 presence. More detailed inspection of dTG curves in Fig. 4b indicates that decomposition processes occurred in four steps. For the sample PPy/TiO_2 270, the initial decrease in mass by 3 mass% up to 120 °C is due to the moisture loss. The next two steps are identified at about 250 and 380 °C indicating the degradation of low molecular weight polymer and oligomers, mass loss of 10%. The degradation of PPy of higher molecular weight occurred at about 680 °C (loss of about 10 mass%). and it is attributed to enhanced crystallinity and cross-linking of the polymer chains. Defects in the PPy structure and cross-linking of the polymer chains caused a creation of one plus charge per 3–4 pyrrole rings, which is counter balanced by the building of an oxidant anion into

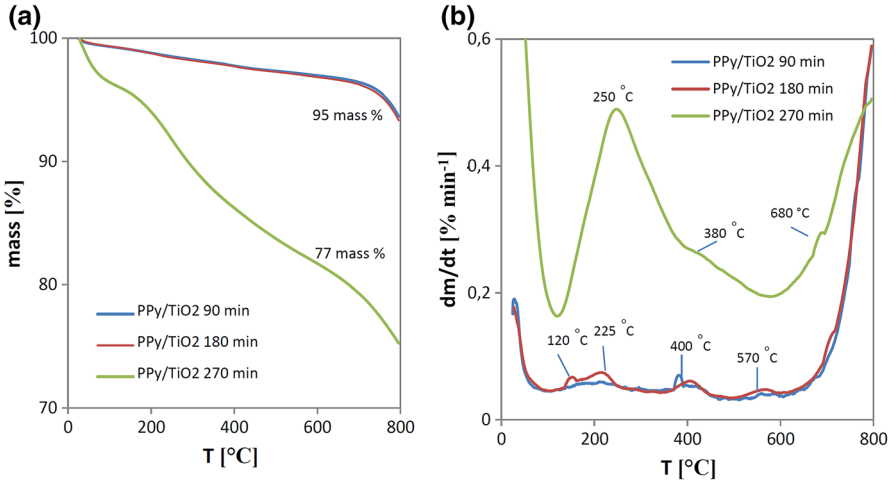

Fig. 4 **a** TG and **b** dTG curves of synthesized PPy/TiO_2 composites

the PPy structure [18–20]. For the samples PPy/TiO_2 90 and 180 very similar decomposition process is observed, but the presence of PPy polymer is in significant lower concentration (about 5 mass% as seen from char residue). Further on, TiO_2 nanoparticles can have "active" sites of different catalytic ability that can induce and initiate the thermal decomposition of PPy. However, the effect of different TiO_2 active sites can be neglected as it is assumed that impact on the degradation rate mainly has the concentration and chemical structure of PPy on TiO_2 surface. So, Fig. 4b shows that PPy/TiO_2 270 presented the highest degradation rate of 0.48% min^{-1} while the other two composites exhibit significant low degradation rate of the 0.07% min^{-1}.

UV–Vis spectroscopy

In Fig. 5a UV–Vis absorbance spectra of pure TiO_2 and PPy/TiO_2 composites are presented to compare and establish their photocatalytic activity in the visible light region. These spectra showed one strong band at 250 nm regarding the TiO_2 absorption and two broad bands, centered approximately at 480 and 750 nm regarding PPy, Fig. 5b). The bands at 480 and 750 nm are assigned to doped PPy due to polaron and bipolaron band transitions [21, 22]. Thereafter in the range from 400 till 550 nm, the absorption peak indicates the polaron transitions, which is ascribed to the transition from the valence band to the antibonding polaron state. Instead of peak at 750 nm in spectrum continuous absorption is noticed indicating the formation of polaron, bipolaron transitions for polypyrrole and can be called free carrier band [23]. This has been assigned to –NH– species that are aggregated during doping and are responsible for the interactions of TiO_2 and polymer. The spectra reveal that the absorption in the visible light region is much higher for the composites PPy/TiO_2 than for the pure TiO_2. The interaction between the doped PPy and particular N–Ti^{2+} was the

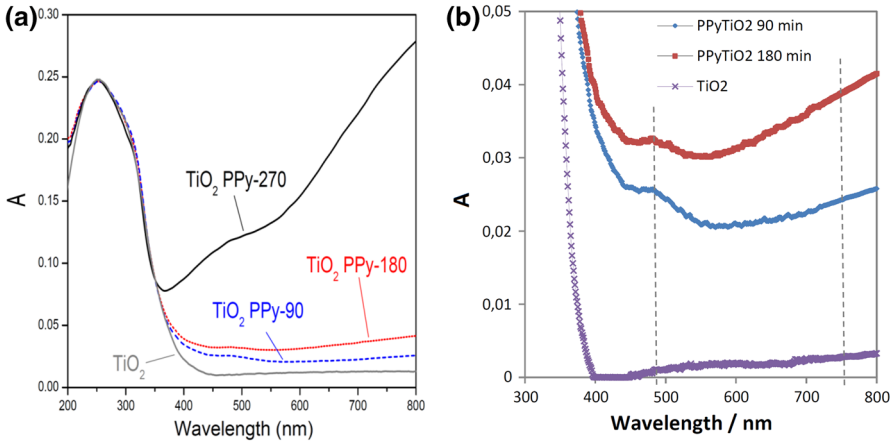

Fig. 5 UV–Vis spectra of TiO_2 and synthesized PPy/TiO_2 composites

key to the extension of the active spectrum under visible light irradiation. It can be noticed that the absorption in the visible region increases with the prolonged polymerization time due to the highest concentration of PPy on the surface of TiO_2 as indicated by TG analysis. This results shows that PPy modification of TiO_2 enables the shift of TiO_2 photograph response into the visible light region. Generally, conducting polymers have a broad UV–Vis adsorption band, due to the wide distribution of conjugated chain length of conducting polymers.

SEM and TEM analysis

The morphology study of PPy/TiO_2 composites has also been carried out by SEM and TEM, presented in Figs. 6 and 7. The observations of morphology based on SEM clearly revealed aggregates with a diameter of around 10 µm for PPy/TiO_2 90 and around 20 µm for PPy/TiO_2 180. SEM and TEM analysis of PPy/TiO_2 270

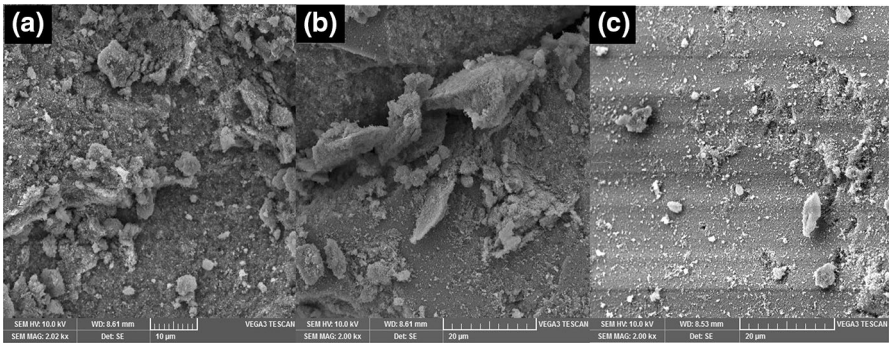

Fig. 6 SEM micrographs of composites at magnification ×2000: **a** PPy/TiO_2 90, **b** PPy/TiO_2 180 and **c** PPy/TiO_2 270 composites

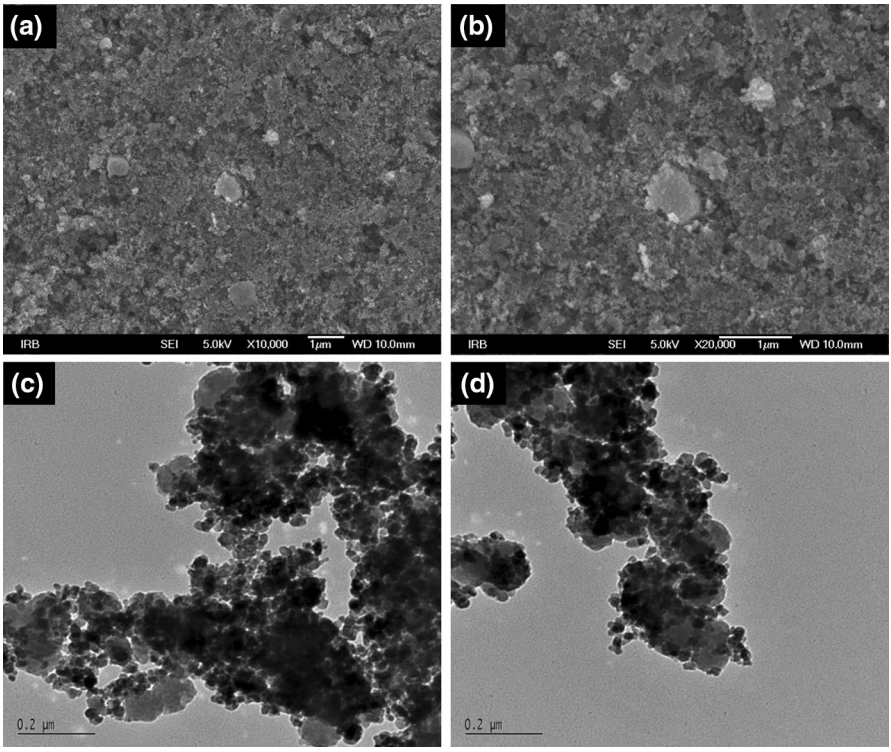

Fig. 7 PPy/TiO_2 270 composites, SEM micrographs: **a** magnification 10,000, **b** magnification 20,000, TEM micrographs: **c** and **d**

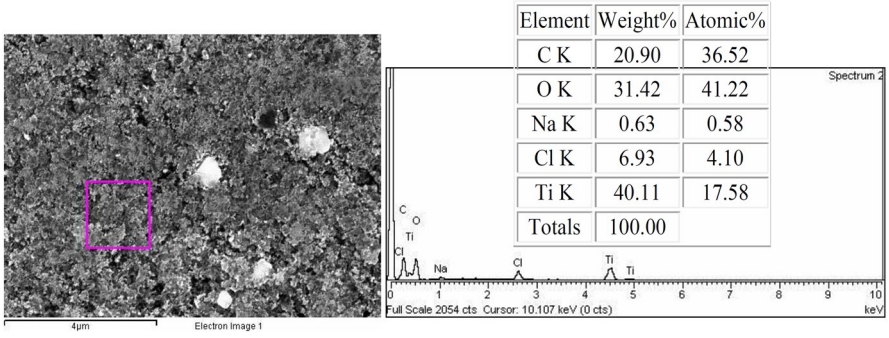

Fig. 8 EDS analysis of PPy/TiO_2 270 composites

composite reveals the absence of aggregates showing more uniform morphology due to the presence of the particles of nanometer dimensions (the size of the particles is between 10 and 20 nm), Figs. 6 and 7. Thus, it can be concluded that concentration of PPy in composite strongly affected the morphology due to higher interaction between PPy and TiO_2 as observed for PPy/TiO_2 270. Furthermore, EDS analysis

(Fig. 8) shows the presence of the titanium (40%), oxygen (31%) and carbon (21%) in PPy/TiO_2 composite. In addition, there is a very small concentration of sodium (0.6%) from sodium chloride and chlorine (6.93%), which originates from oxidant ferric chloride indicating high degree of conductivity of PPy polymer.

Photocatalysis and effect of pH value of the solution

Photocatalytic activity of synthesized PPy/TiO_2 composites was examined in a process of degradation of azo dye Reactive Red 45 (RR45) in a waste water. In order to determine the optimal conditions for the photocatalysis the photocatalytic performance with PPy/TiO_2 90 composite photocatalyst under UVA light irradiation was performed at different pH values. The results show significant difference in adsorption process that was carried out in the dark for 30 min to achieve adsorption–desorption equilibrium. Results indicate that at pH 4 (acid medium) the catalyst strongly adsorbs RR45 dye (more than 80%). Such strong dye adsorption of some composite photocatalysts is explained by chemical interaction of negative anionic dye (SO_3^-) (Fig. 9) with the positively charged TiO_2 and PPy backbone in acid media [24].

At the beginning of photocatalysis desorption takes place due too high concentration of dye on the catalyst surface. When the media of photocatalysis is alkaline (pH = 11), catalytic process was completely inefficient, only 3.5% of RR45 dye was degraded in 90 min. The results indicate opposite behavior from that in acid media. The best photocatalytic activity of PPy/TiO_2 composite was obtained at pH 6.6 (almost neutral media) because the adsorption of the dye was very low (8%) and the photocatalytic process was efficient due to dye degradation of 70% in 90 min, Fig. 10a).

Furthermore, for these processes the kinetics was also considered and apparent rate constant kapp of photodegradation of RR45 was determined using Langmuir–Hinshelwood model for the degradation of organic pollutant in waste water with semiconducting oxide, $\ln(C_0/C_t) = k_{app}\ t$, where k_{app} is apparent rate constant, C_0 and C_t are concentration of dye after darkness adsorption of 30 min and concentration of dye at time t [25]. In Fig. 10b it is seen that the relationship between the illumination time and degradation rate of RR45 dye under UVA light gives linear correlation and the plot of $\ln(C_0/C_t)$ versus time suggests a pseudo-first-order reaction. The catalytic activity of composite photocatalyst in different media was validated comparing the apparent rate constants (k_{app}), presented in Table 1, and it is

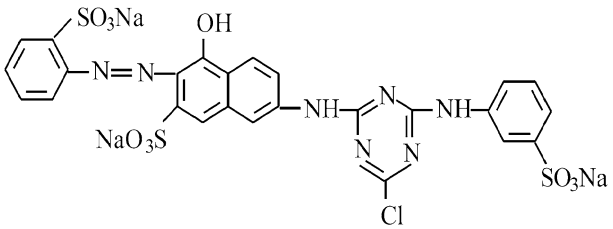

Fig. 9 Molecular structure of azo dye Reactive Red 45 (RR45)

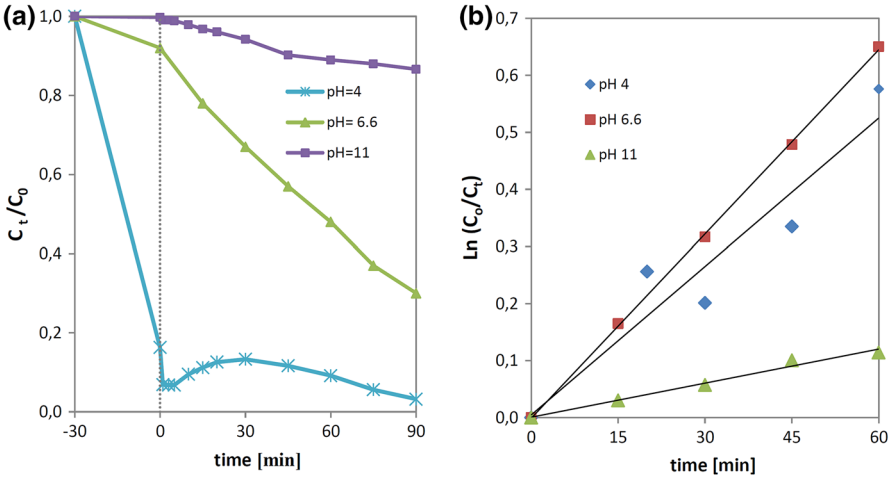

Fig. 10 **a** Concentration ratio C_t/C_0 versus time of photocatalysis, **b** the kinetic curves of RR45 dye degradation at different pH values with PPy/TiO_2 90 catalyst under UVA irradiation ($\gamma_{cat} = 1$ g dm^{-3}, $\gamma_{(RR45)} = 30$ mg dm^{-3})

Table 1 Apparent rate constants (k_{app}) of RR45 dye degradation and linear regression coefficients from plot of $\ln(C_0/C_t) - t$ for tested samples under UVA irradiation

PPy/TiO_2 90 min	pH 4	pH 6.6	pH 11
k_{app} (min^{-1})	0.0097	0.0108	0.0020
R^2	0.9067	0.9996	0.9838

observed that k_{app} has the highest value at pH 6.6 (0.0108 min^{-1}). It was concluded that pH value of 6.6 is the most suitable option, and this pH value is the most environmentally friendly because it does not demand further neutralization of water at the end of purification process. In this study all further photocatalytic experiments were performed at pH 6.6.

Photocatalytic validation of PPy/TiO_2 composites

In Fig. 11a are presented the results for the photocatalytic process under UV light irradiation, using photocatalysts PPy/TiO_2 synthesized for 90, 180 and 270 min. From the results, it is apparent that the most effective composite catalyst during the decomposition of Reactive Red 45 in waste water was PPy/TiO_2 270 synthesized for 270 min. It can be concluded that this composite catalyst has almost the same efficiency as the pure TiO_2 according to the discoloration achieved after 60 min (Table 2), which is 96% for TiO_2 and 98% for PPy/TiO_2 270 catalyst.

It is well seen that TiO_2 exhibits higher rate of degradation in the first 45 min and higher degradation rate of RR45 is confirmed by apparent constant rate (k_{app})

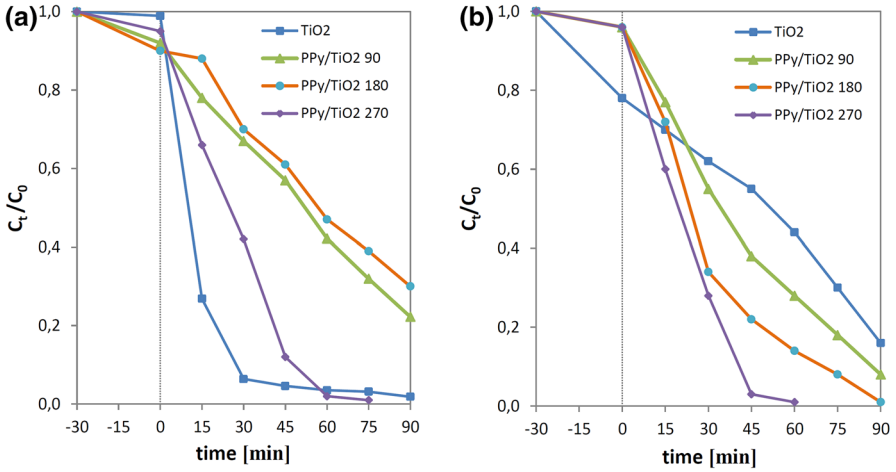

Fig. 11 Concentration ratio C_t/C_0 during photocatalysis with different catalysts: **a** under UVA and **b** under solar irradiation ($\gamma_{cat}=1$ g dm^{-3}, $\gamma_{(RR45)}=30$ mg dm^{-3})

Table 2 Comparison of photocatalytic efficiency of used catalysts under UVA and solar irradiation after 60 min of the photocatalysis

Catalyst	Discoloration/%
Photocatalysis with UVA irradiation ($t=60$ min)	
TiO_2	96
PPy/TiO_2 90	43
PPy/TiO_2 180	39
PPy/TiO_2 270	98
Photocatalysis with solar irradiation ($t=60$ min)	
TiO_2	56
PPy/TiO_2 90	70
PPy/TiO_2 180	86
PPy/TiO_2 270	99

obtained by Langmuir–Hinshelwood model, Fig. 12a and Table 2. Such results are expected due to UVA irradiation under which TiO_2 is one of the most effective catalysts. The high photocatalytic efficiency of PPy/TiO_2 270 catalyst compared to pure TiO_2 can be explained by the fact that a very small fraction of polypyrrole on the TiO_2 surface can prevent the aggregation of its nanoparticles. When the specific surface area of the catalyst is increased, the more active space is available for the contact with pollutants because the photodegradation takes place at the surface of catalyst [26].

Furthermore, the photocatalysis process was also performed under the solar irradiation for the same PPy/TiO_2 composite catalysts, Fig. 11b. From the results it is seen that all composite photocatalysts exhibit higher discoloration than the

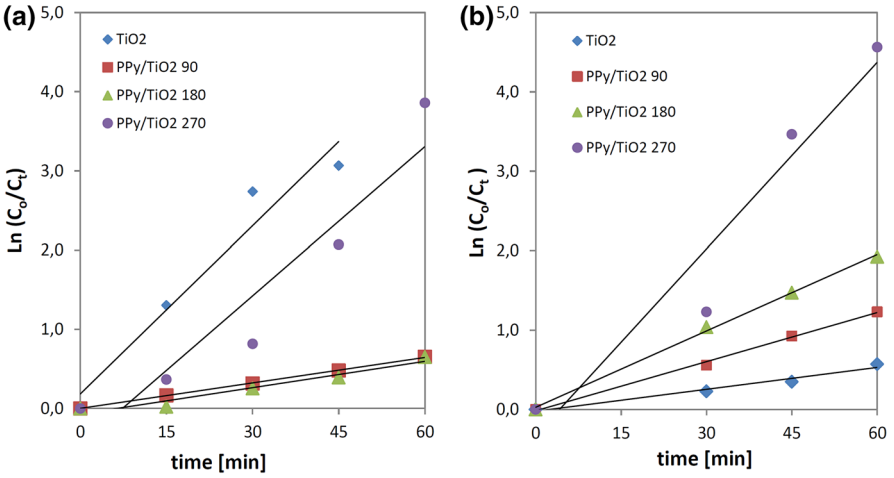

Fig. 12 Kinetic curves of RR45 dye degradation **a** under UVA and **b** under solar irradiation versus time of photocatalysis with different catalysts

pure TiO_2 indicating very good photosensitivity under Vis light irradiation due to synergistic effect of PPy–TiO_2. Especially high photocatalytic efficiency of the PPy/TiO_2 270 composite photocatalyst was observed because the complete discoloration (99%) of waste water is achieved in only 60 min, Table 2. Another two composites catalysts show also very good removal of RR45 from waste water due to discoloration of 86 and 70% in 60 min. It can be concluded that prepared composite photocatalysts are photosensitive as it was confirmed by the UV/Vis spectrum (Fig. 5). This further indicates that the strong interactions between the TiO_2 and polypyrrole are present on the interface, so then conjugated polypyrrole structure and its conductivity can easily contribute to the injection of electron into conductive band of the TiO_2 [27]. This is based on the theory that when PPy/TiO2 composite is irradiated by sunlight, both TiO_2 and PPy absorb the photons at their interface and then charge separation occurs. Since, when the adsorbed energy is higher than the band gap, the electrons of PPy from the lowest unoccupied molecular orbital level are injected to conductive band of TiO_2. After such activation, there occurs basic mechanism of photocatalytic degradation of organic pollutant in waste water by TiO_2. When TiO_2 nanoparticles are irradiated by UVA light, they generate electron–hole pairs that react with water and yield hydroxyl ($OH^{\cdot}$) and superoxide radicals ($O_2^{-\cdot}$) to oxidize the organic molecules of pollutant [2, 4].

Table 2 shows a comparison of photocatalyst efficiency results under UVA and solar light irradiation after 60 min of photocatalysis are presented. TiO_2 catalyst shows significantly higher photocatalitic efficiency under UVA irradiation because 94.7% of the RR45 pollutant in the 45 min was degraded. At the same time PPy/TiO_2 90 and 180 photocatalysts removed less than 50% of dye. Under the solar light, the TiO_2 efficiency is much lower, but the composites' efficiency increases. This is well seen from the decomposition rate of RR45 during solar

Table 3 Apparent rate constants (k_{app}) of RR45 dye degradation and linear regression coefficients from plot of $\ln(C_0/C_t) - t$ for tested catalysts under UVA and solar irradiation

	PPy/TiO_2 90	PPy/TiO_2 180	PPy/TiO_2 270	TiO_2
UVA irradiation				
k_{app} (min^{-1})	0.0108	0.0111	0.0628	0.0790
R^2	0.9996	0.9486	0.9345	0.9474
Solar irradiation				
k_{app} (min^{-1})	0.0207	0.0321	0.0783	0.0092
R^2	0.9968	0.9981	0.9349	0.9725

photocatalysis since the apparent constant rate (k_{app}) was determined and is presented in Table 3 and Fig. 12 and can be seen that PPy/TiO_2 270 composite has the highest rate. Furthermore, all k_{app} of composite sample are higher under solar irradiation.

The results indicate that by prolonged time of synthesis and a higher fraction of polypyrrole of suitable molecular structure in the composite contribute to the efficiency of the photocatalyst. This, however, does not mean that the further prolongation of synthesis time would increase the photocatalytic power of the composite. An excessive amount of polypyrrole (thicker than the monomolecular polypyrrole layer) on TiO_2 surface would actually reduce its photocatalytic activity because the "thick" layer of polypyrrole, with visible light, could no longer be in such close contact with TiO_2. In that case the transfer of electrons to the TiO_2 conductive band would be difficult and its photocatalytic power would be reduced. It is evident that photocatalytic activity significantly depends on PPy conductive polymer presence in composite. The properties of conductive polymer primarily depend on the oxidation of the polymer during the synthesis, on monomer/oxidant ratio and the type of used oxidant as well as the temperature. For example, the synergetic effect between TiO_2 and PPy conductive polymer in nanocomposite strongly depends on charge mobility in polymer [20].

Total organic carbon

In Table 4 are given the results of the total organic carbon (TOC) determined at the end of each photocatalytic process in comparison with the TOC value of the pure RR45 dye before photocatalysis. It is apparent that TiO_2 and PPy/TiO_2 270 composites are exceptionally efficient photocatalysts under UVA light irradiation because TOC values are significantly reduced after photocatalysis. It is seen that 65.3 and 80.1% of RR45 dye was completely removed from the waste water, respectively. Under the solar irradiation, the efficiency of all studied PPy/TiO_2 composites was higher than under UVA light indicating synergistic effect of PPy and TiO_2 since the pure TiO_2 shows low photocatalytic efficiency. From the results, it is seen that the mineralization of RR45 azo dye is even higher under solar irradiation when composites are used as photocatalysts. These results are consistent with the results of photocatalytic activity where the most efficient

Table 4 Comparison of TOC values and percentage of RR45 dye removal under UVA and solar irradiation

	TOC mg dm^{-3}	RR45 dye mineralization %
Reactive Red 45 (before photocatalysis)	9.16	0
Photocatalysis with UVA irradiation		
TiO_2	3.18	65.3
PPy/TiO_2 90	7.43	18.9
PPy/TiO_2 180	7.18	21.6
PPy/TiO_2 270	1.82	80.1
Photocatalysis with solar irradiation		
TiO_2	6.63	27.6
PPy/TiO_2 90	7.38	19.4
PPy/TiO_2 180	6.10	33.4
PPy/TiO_2 270	1.69	81.6

photocatalyst is proved to be PPy/TiO_2 270 under the solar irradiation. TOC denotes the mineralization of the dye, i.e., its decomposition on the CO_2 and H_2O indicating the removal of the RR45 dye and its degradation products. PPy/TiO_2 270 photocatalyst showed effective activity in decolorization process and in the removal of total organic carbon under simulated solar radiation.

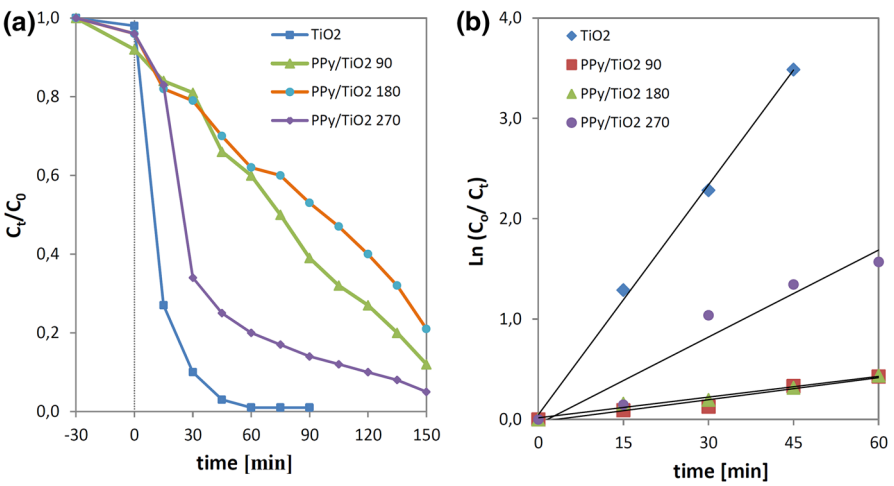

Fig. 13 **a** concentration ratio C_t/C_0 versus time of photocatalysis, **b** the kinetic curves of RR45 dye degradation with different catalysts under UVA irradiation in the second photocatalysis cycle ($\gamma_{cat} = 1$ g dm^{-3}, $\gamma_{(RR45)} = 30$ mg dm^{-3})

Table 5 Apparent rate constants (k_{app}) of RR45 dye degradation and linear regression coefficients from plot of $\ln(C_0/C_t) - t$ for tested samples under UVA irradiation for the second photocatalysis cycle

	PPy/TiO_2 90	PPy/TiO_2 180	PPy/TiO_2 270	TiO_2
k_{app} (min^{-1})	0.0073	0.0069	0.0289	0.0756
R^2	0.9515	0.9758	0.9352	0.9988

Table 6 Comparison of photocatalytic efficiency of catalysts under UVA irradiation after 60 and 90 min of the photocatalysis

Second cycle of photocatalysis with UVA irradiation		
Catalysts	Discoloration/%	
	($t = 60$ min)	($t = 90$ min)
TiO_2	98	98
PPy/TiO_2 90	38	60
PPy/TiO_2 180	35	47
PPy/TiO_2 270	80	83

Stability of photocatalyst

Photocatalytic activity of prepared composite photocatalysts was also investigated in the second photocatalytic cycle under UVA light to examine their reuse and stability during the catalytic process. After the first photocatalytic cycle, the photocatalysts were not reactivated or additionally treated; they were only dried and reused. The results are given in Fig. 13 and in Tables 5 and 6. It is apparent that photocatalyst' efficiency slightly decreases after the second cycle, but their efficiency is satisfactory, although photocatalysts required longer time to complete photocatalysis,

The decomposition rate of RR45 during photocatalysis was also determined and is presented in Table 5. From the apparent constant rate (k_{app}) it can be seen that the decomposition in first 60 min is slowed down for the composite catalysts but not for TiO_2. For example, in the second cycle PPy/TiO_2 270 removed 80% of dye in 60 min while in the first cycle it removed 98%. This is explained by saturation of the catalyst surface during the second cycle and by aggregation of the catalyst particles [26]. Due to a very good activity of PPy/TiO_2 composite photocatalysts under UVA light during the second consecutive photocatalytic cycle, they are recognized as stable catalysts.

Conclusions

PPy TiO_2 photocatalysts were successfully prepared by PPy polymerization in the presence of TiO_2. It was found that prepared photocatalysts are very efficient both under the UVA and solar irradiation due to the synergistic effect of PPy and TiO_2 during photocatalysis, i.e., because of TiO_2 sensitization with PPy. The fraction of

polypyrrole on the TiO_2 surface prevents the aggregation of TiO_2 nanoparticles and enables efficient photocatalytic action of the composite system. It is shown that pH value 6.6 was the optimal one for the successful process of Reactive Red 45 azo dye photocatalytic degradation. Photocatalyst PPy TiO_2 270 is the most efficient photocatalyst for this photocatalytic process due to its good absorbtion in the visible light region. Used photocatalysts have particles of nanodimensions, what is also a contribution to the successful photocatalysis because the specific surface area of the catalyst is increased so the more active space is available for the contact with pollutants. The results also show that TOC value is significantly decreased after the photocatalysis, which proves the efficiency of the process. Prepared composite samples are recognized as stable catalysts after second consecutive photocatalytic cycle.

Finally, it can be concluded that TiO_2 modification with PPy can serve as a very efficient method for the improvement of TiO_2 photocatalytic performance under visible light.

Acknowledgements This work was financially supported by Croatian Science Foundation (Hrvatska zaklada za znanost, HRZZ) through the research project "Development of Photocatalytic Polymer Nanocomposites for Wastewater Treatment" DePoNPhoto, Project Number 5092.

References

1. Lang X, Chen X, Zhao J (2014) Heterogeneous visible light photocatalysis for selective organic transformations. Chem Soc Rev 43:473–486. https://doi.org/10.1039/c3cs60188a
2. Serpone N, Emeline AV (2012) Semiconductor photocatalysis—past, present, and future outlook. J Phys Chem Lett 3:673–677. https://doi.org/10.1021/jz300071j
3. Jing L, Zhou W, Tiana G, Fu H (2013) Surface tuning for oxide-based nanomaterials as efficient photocatalysts. Chem Soc Rev 42:9509–9549. https://doi.org/10.1039/C3CS60176E
4. Pelaez M et al (2012) A review on the visible light active titanium dioxide photocatalysts for environmental applications. Appl Catal B 125:331–349. https://doi.org/10.1016/j.apcatb.2012.05.036
5. Plass R, Pelet S, Krueger J, Gratzel M (2002) Quantum dot sensitization of organic–inorganic hybrid solar cells. J Phys Chem B 106:7578–7583. https://doi.org/10.1021/jp020453l
6. Park JH, Kim S, Bard A (2006) Novel carbon-doped TiO_2 nanotube arrays with high aspect ratios for efficient solar water splitting. J Nano Lett 6:24–28. https://doi.org/10.1021/nl051807y
7. Umebayashi T, Yamaki T, Itoh H, Asai K (2002) Band gap narrowing of titanium dioxide by sulfur doping. Appl Phys Lett 81:454–456. https://doi.org/10.1063/1.1493647
8. Asahi R, Morikawa T, Ohwaki T, Aoki K, Taga Y (2001) Visible-light photocatalysis in nitrogen-doped titanium oxides. Science 293:269–271. https://doi.org/10.1126/science.1061051
9. Chen X, Liu L, Yu PY, Mao SS (2011) Increasing solar absorption for photocatalysis with black hydrogenated titanium dioxide nanocrystals. Science 331:746–750. https://doi.org/10.1126/science.1200448
10. Cobo I, Li M, Sumerlin BS, Sébastien Perrier S (2015) Smart hybrid materials by conjugation of responsive polymers to biomacromolecules. Nat Mater 14:143–159. https://doi.org/10.1038/nmat4106
11. Lutteroti L. Material analysis using diffraction (MAUD). General diffraction/reflectivity analysis program. http://www.ing.unitn.it/~maud/index.html. Accessed 1 June 2017
12. López R, Gómez R, Oros S (2011) Photophysical and photocatalytic properties of TiO_2–Cr sol–gel prepared semiconductors. Catal Today 166:159–165. https://doi.org/10.1016/j.cattod.2011.01.010
13. Jeeju PP, Varma SJ, Puthampadath AFS, Sajimol AM, Jayalekshmi S (2012) Novel polypyrrole films with excellent crystallinity and good thermal stability Mater. Chem Phys 134:803–808. https://doi.org/10.1016/j.matchemphys.2012.03.072
14. Dai T, Yang X, Lu Y (2007) Conductive composites of polypyrrole and sulfonic-functionalized silica spheres. Mater Lett 61:3142–3145. https://doi.org/10.1016/j.matlet.2006.11.012

15. Pine SH, Hendrickson JB, Cram DJ, Hammond GS (1980) Organic chemistry, 4th edn. McGraw-Hill Kogakusha LTD, Tokyo
16. Turcu RP, Bica D, Vekas L, Aldea N, Macovei D, Nan A, Pana O, Marinica O, Grecu R, Pop CVL (2006) Synthesis and characterization of nanostructured polypyrrole-magnetic particles hybrid material. Romanian Rep Phys 58:359–367
17. Klug HP, Alexander LE (1974) X-ray diffraction procedures for polycrystalline and amorphous materials, 2nd edn. Wiley, New York
18. Metin A, Cilgi GK, Kuru FD, Cetisli H (2013) Thermal decomposition kinetics of polypyrrole and its star shaped copolymer. J Therm Anal Calorim 111:1627–1632. https://doi.org/10.1007/s10973-012-2351-1
19. Jakab E, Mészáros E, Omastová M (2007) Thermal decomposition of polypyrroles. J Therm Anal Calorim 88:515–521
20. Bhaumik M, McCrindle R, Maity A (2013) Efficient removal of Congo red from aqueous solutions by adsorption onto interconnected polypyrrole–polyaniline nanofibres. Chem Eng J 228:506–515. https://doi.org/10.1016/j.cej.2013.05.026
21. Wang ZL, Kong XY, Ding Y, Gao P, Hughes WL, Yang R, Zhang Y (2004) Semiconducting and piezoelectric oxide nanostructures induced by polar surfaces. Adv Funct Mater 14:943–956. https://doi.org/10.1002/adfm.200400180
22. Bof Bufon CC, Vollmer J, Heinzel T, Espindola P, John H, Heinze J (2005) Relationship between chain length, disorder, and resistivity in polypyrrole films. J Phys Chem B 109:19191–19199. https://doi.org/10.1021/jp053516j
23. Abdulla HS, Abbo AI (2012) Optical and electrical properties of thin films of polyaniline and polypyrrole. Int J Electrochem Sci 7:10666–10678
24. Mahanta D, Madras G, Radhakrishnan S, Patil S (2008) Adsorption of sulfonated dyes by polyaniline emeraldine salt and its kinetics. J Phys Chem B 112(33):10153–10157. https://doi.org/10.1021/jp803903x
25. Sadollahkhani A, Kazeminezhad I, Lu J, Nur O, Hultman L, Willander M (2014) Synthesis, structural characterization and photocatalytic application of ZnO@ZnS core–shell nanoparticles. RSC Adv 4:36940–36950. https://doi.org/10.1039/C4RA05247A
26. Luo Q, Li X, Wang D, Wang Y, An J (2011) Photocatalytic activity of polypyrrole/TiO_2 nanocomposites under visible and UV light. J Mater Sci 46:1646–1654
27. Ghosh S, Kouamé NA, Ramos L, Remita S, Dazzi A, Deniset-Besseau A, Beaunier P, Goubard F, Aubert PH, Remita H (2015) Conducting polymer nanostructures for photocatalysis under visible light. Nat Mater 14:505–511. https://doi.org/10.1038/nmat4220